PAPER

CrossMark
click for updates

Efficient synthesis of 2,5-dihydroxymethylfuran and 2,5-dimethylfuran from 5-hydroxymethylfurfural using mineral-derived Cu catalysts as versatile catalysts†

Yifeng Zhu,‡[ab] Xiao Kong,‡[ab] Hongyan Zheng,[c] Guoqiang Ding,[c] Yulei Zhu*[ac] and Yong-Wang Li[ac]

Selective conversion of 5-hydroxymethylfurfural (HMF) can produce sustainable fuels and chemicals. Herein, Cu–ZnO catalysts derived from minerals (malachite, rosasite and aurichalcite) were employed for selective hydrogenation of HMF for the first time. High yields of 2,5-dihydroxymethylfuran (~99.1%) and 2,5-dimethylfuran (~91.8%) were obtained tunably over the catalyst with a Cu/Zn molar ratio of 2, due to the well-dispersed metal sites tailored by mineral precursors, well-controlled surface sites and optimized reaction conditions. The relationship between catalytic performance and catalyst properties was elucidated by characterization based on the composition and the structural and surface properties, and catalytic tests. The catalyst can also be extended to selective hydrogenation of other bio-derived molecules (furfural and 5-methylfurfural) to target products. The construction of mineral-derived Cu–ZnO catalysts and the revelation of the structure–performance relationship can be applied to further rational design and functionalization of non-noble Cu catalysts for selective conversion of bio-derived compounds.

Introduction

Growing interest has been paid to utilization of renewable biomass to replace the diminishing fossil resources for energy and chemical supply. 5-Hydroxymethylfurfural (HMF) is an important platform chemical which could be facilely obtained from renewable biomass resources (*e.g.*, cellulose, glucose and fructose) using acid catalysts.[1,2] It contains many functional groups including C=O, C–O, C=C and the furan ring, which allow its hydrogenation to various products (*e.g.*, 2,5-dihydroxymethylfuran (DHMF), 2,5-dimethylfuran (DMF), 2,5-dihydroxymethyltetrahydrofuran (DHMTHF) and 2,5-dimethyltetrahydrofuran (DMTHF)).[1] Among these derivatives, DHMF and DMF attract great interest. In this paper, we aim at tunable synthesis of DHMF and DMF over the same non-noble catalyst, which is challenging but valuable work for both academic and industrial purposes.

DHMF is a promising diol, which could be either directly used for producing shape memory and self-healing polymers or used for synthesis of 1,6-hexanediol which is also an important polymer precursor.[3–5] Besides, it can also be employed for production of intermediates of drugs and crown ethers.[6] Selective hydrogenation of HMF to DHMF is a hydrogenation reaction of the aldehyde group. The side reactions involving C=C, C–O and furan ring hydrogenation should be suppressed.

DMF is an alternative fuel with high energy density (30 kJ cm⁻³) and octane number (RON = 119), holding great potential to substitute for petroleum-based gasoline.[7] As a diene, DMF can also be converted to valuable benzene-based chemicals *via* Diels–Alder reactions.[8,9] Production of DMF from HMF involves C=O hydrogenation and C–O hydrogenolysis reactions, while C=C hydrogenation and ring-opening reactions need to be avoided.

Previous studies on selective hydrogenation of HMF to DHMF and DMF were mainly performed on noble metal catalysts, which is a great impediment to industrial applications. For DHMF synthesis, Alamillo *et al.*[10] studied supported Ru, Pd and Pt catalysts for HMF hydrogenation, of which Ru was the most active metal with a yield of 81–94%. An Au/Al₂O₃ catalyst was proposed for DHMF production with 96% yield at 140 °C and 3.8 MPa.[11] Other catalysts were also reported, including Pt/MCM-41,[6] Pd/C[12] and Ir–ReOₓ/SiO₂.[13] For DMF

[a] State Key Laboratory of Coal Conversion, Institute of Coal Chemistry, Chinese Academy of Sciences, Taiyuan 030001, PR China. E-mail: zhuyulei@sxicc.ac.cn; Fax: +86 351 7560668; Tel: +86 351 7117097
[b] University of Chinese Academy of Sciences, Beijing 100049, PR China
[c] Synfuels China Co. Ltd, Beijing, 101407, PR China
† Electronic supplementary information (ESI) available: Table S1 and Fig. S1–S3. See DOI: 10.1039/c5cy00700c
‡ These authors contributed equally.

This journal is © The Royal Society of Chemistry 2015

production, Dumesic *et al.*[7] reported for the first time a Ru–Cu catalyst with a yield of 76–79%. Many subsequent reports were also mainly conducted on noble metals (*e.g.*, Pd,[12] Ru,[14,15] and Pt[16]). However, few reports on the development of non-noble substitutes existed, due to their low reactivity. Ni-based (*e.g.*, RANEY® Ni,[17] Ni/Al$_2$O$_3$ (ref. 18) and Ni–W$_2$C/AC[19]) catalysts emerged for DMF synthesis; on the other hand, they were difficult to be employed in DHMF synthesis due to the strong C═C hydrogenation ability of Ni. Recently, Cu/MgO/Al$_2$O$_3$ and Ru-modified Cu/MgO/Al$_2$O$_3$ catalysts derived from hydrotalcite have been employed in synthesis of DHMF and DMF.[20,21] Nevertheless, the development of non-noble catalysts still requires considerable effort prior to their commercial applications.

Another challenge for HMF hydrogenation is the poor selectivity to products due to the presence of many functional groups of HMF, DHMF and DMF. To obtain high yields of DHMF/DMF, the efficiency of C═O hydrogenation and/or C–O hydrogenolysis needs to be promoted. Commonly used noble metal (*e.g.*, Ru, Pd) and Ni catalysts are good candidates, whereas the saturation of the furan ring easily proceeds over these catalysts with strong C═C hydrogenation abilities.[17,18,22] For example, DHMF yield would be reduced by the formation of DHMTHF over RANEY® Ni and Ni–Al$_2$O$_3$ catalysts.[17,18] Ru-modified Cu/MgO/Al$_2$O$_3$ catalysts were reported for HMF hydrogenation with high reactivity.[20] However, Ru sites would also promote C═C hydrogenation reactions and lower the DMF yield. Control of surface acidity is also crucial. An appropriate amount of acid sites and high reaction temperature would facilitate DMF formation *via* hydrogenolysis of CH$_2$OH groups, whereas CH$_2$OH groups need to be preserved for DHMF production.[20,23] Besides, excessive amounts of acid sites would catalyze the ring-opening reactions and etherification, and thus lower the selectivity to DHMF and DMF.[10] Thus, the choice of metal, suitable surface acidity and reaction conditions are important for tunable synthesis of DHMF and DMF from HMF, in particular over the same catalyst. Cu catalysts are one of the best materials for selective hydrogenation, due to their high reactivity to C═O and C–O bonds and relatively low reactivity to C═C and C–C bonds.[24–26] ZnO, as a catalyst support, has moderate surface acidity, facilitating the possibility of tunable synthesis of DHMF and DMF.

In view of the above problems, rational design of efficient non-noble catalysts based on the composition, structure and properties of materials is a prerequisite. Herein, we reported that mineral-derived Cu–ZnO catalysts (malachite, rosasite and aurichalcite) can efficiently catalyze the selective conversion of HMF into either DHMF or DMF for the first time (Scheme 1). This work addresses at least the following desired features: (1) highly selective and tunable synthesis of DHMF and DMF over the non-noble Cu catalysts was realized; (2) highly dispersed Cu sites and high reactivity of the catalysts can be obtained by using Cu–Zn binary minerals as precursors; (3) the revelation of the structure–performance relationship can facilitate further rational development of active Cu catalysts. Besides, the mineral-derived Cu–ZnO
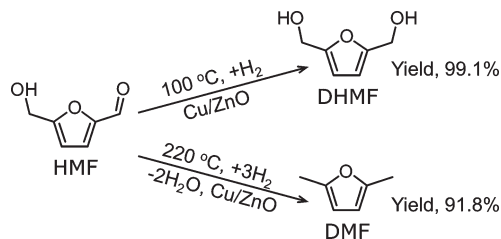
Scheme 1 Tunable synthesis of DHMF and DMF from HMF hydrogenation.

catalysts can be extended to selective conversion of other bio-derived molecules (furfural and 5-methylfurfural), demonstrating the great potential of these catalysts for biomass utilization.

Experimental section

Preparation and evaluation

Copper nitrate trihydrate, zinc nitrate hexahydrate and sodium carbonate were purchased from Sinopharm Co., Ltd. and used as-received. The catalyst precursors were prepared by a facile constant-pH co-precipitation method.[27] A solution containing copper nitrate and zinc nitrate with preset Cu/Zn molar ratios was prepared. An aqueous solution of Na$_2$CO$_3$ (2 mol L^{-1}) was employed as the precipitant. The two solutions were then simultaneously introduced into a 2 L vessel at 65 °C and a pH of 6.5 ± 0.2. After precipitation, the suspension was aged for 150 min in the mother liquor and then washed and dried at 65 °C for 12 h, followed by calcination at 350 °C for 4 h in air. The resulting samples were denoted as CuZn-*x*, of which *x* indicates the molar ratio of Cu/Zn. For comparison, the catalyst without Zn^{2+} added was denoted as CuZn-inf, of which inf means infinite.

Prior to the tests, the catalysts were *ex situ* reduced in a tube reactor under H$_2$ atmosphere at 250 °C (heating rate of 0.5 °C min^{-1}) for 2 h. The tests were performed in an autoclave reactor (100 mL) after the *ex situ* reduction of the catalysts. Typically, 1.5 g of HMF (Shanghai Demo Pharmaceutical Science and Technology Co., Ltd., 98%), 35 mL of 1,4-dioxane (Sinopharm, AR) and 0.5 g of the catalyst were placed into the reactor. The reactor was then sealed and purged with H$_2$ 5 times. After that, the reactor was filled with H$_2$ at the desired pressure and heated to the objective temperature. After the tests, the products were collected and analyzed by using a GC instrument with an FID.

Characterization

The elemental compositions were determined by inductively coupled plasma-optical emission spectroscopy (ICP, Perkin Elmer Optima 2100DV). XRD experiments were conducted on a Rigaku D/max-2000 diffractometer with Cu Kα radiation operating at 40 kV. The BET surface areas, pore diameters and pore volumes of calcined catalysts were measured *via* N$_2$ physical adsorption at −196 °C using a Micromeritics ASAP 2420 instrument after the samples were degassed at 90 °C for

This journal is © The Royal Society of Chemistry 2015

*Catal. Sci. Technol.*, 2015, **5**, 4208–4217 | **4209**

1 h and at 350 °C for 8 h. H_2 temperature-programmed reduction (TPR) and N_2O titration experiments were performed on a Tianjin XQ TP-5080 instrument equipped with a TCD. The surface acidity of the catalysts was determined by temperature-programmed desorption of ammonia (NH_3-TPD) using a Micromeritics ASAP 2920 instrument and a mass spectrometric detector. The infrared (IR) spectra of the catalysts were obtained by using a Nicolet NEXUS 470 FT-IR spectrometer in the range of 400–4000 cm^{-1} with a resolution of 4 cm^{-1}. The Raman spectra of the samples were recorded using a LabRAM HR800 system equipped with a CCD detector at room temperature. A He–Cd laser with a wavelength of 325 nm was employed as the excitation source with a power of 30 MW. Thermogravimetry (TG) experiments of fresh reduced and used catalysts were performed on a Mettler Toledo TGA/SDTA 851 instrument (air atmosphere and heating rate of 10 °C min^{-1}). Prior to the test, both the fresh reduced and used catalysts were dried in air at 100 °C for 24 h.

Results and discussion

Brief introduction of the precursors

Malachite is a carbonate with a formula of $[Cu_2(CO_3)(OH)_2]$. It contains two crystallographically different CuO_6 octahedral sites which are coordinated to six O atoms of CO_3^{2-} and OH^- ions in a Jahn–Teller distorted octahedron.[28,29] When some Zn^{2+} ions were added (Cu/Zn molar ratio >2.7), single-phase rosasite with a general formula of $[(Cu,Zn)_2(CO_3)(OH)_2]$ can be obtained.[30] Although it has similar composition to malachite, rosasite is not isomorphous with malachite. The main difference between them is the orientation of the Jahn–Teller elongated axes of the CuO_6 octahedra.[31] Addition of higher amounts of Zn^{2+} ions (Cu/Zn molar ratio <2.7) results in the formation of aurichalcite which has a general formula of $[(Cu,Zn)_5(OH)_6(CO_3)_2]$.[29,30] Aurichalcite contains four crystallographically different metal sites (Cu^{2+} and/or Zn^{2+}) in the lattice (denoted as M1, M2, M3 and M4), of which M1 and M2 are coordinated to six O atoms, M3 is coordinated to four O atoms and M4 is located at a five-fold trigonal bipyramid.[28,29] M3 is totally occupied by Zn^{2+} while the others can be occupied by Cu^{2+} and Zn^{2+} with equal probability.[28,32]

Despite the different and complex formulas and structures, malachite, rosasite and aurichalcite minerals can be tunably synthesized simply through a constant-pH co-precipitation method by varying the Cu/Zn molar ratios (Scheme 2).[27] Due to the homogeneous distributions of elements (Cu and Zn) in the minerals and different morphologies, the above minerals are important precursors for construction and meso-/nano-structuring of Cu–ZnO catalysts.[30] Herein, the above minerals were obtained at different preset Cu/Zn molar ratios (1, 2, 3, 4 and infinite). Upon calcination and reduction, highly dispersed Cu–ZnO catalysts with different Cu loadings were obtained which exhibited high performance for tunable production of DHMF (99.1%) and DMF (91.8%) from HMF hydrogenation.
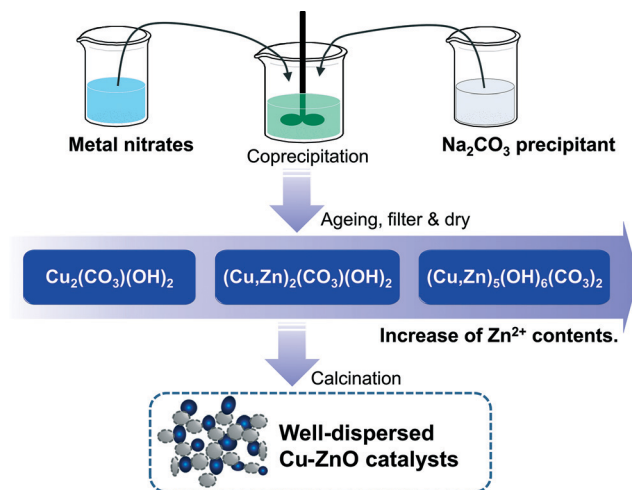
Scheme 2 Synthesis of Cu–ZnO catalysts with mineral precursors using a constant-pH co-precipitation method (pH value was adjusted by controlling the dropping speed).

Moreover, the contents of the active phases and the compositions are highly flexible in a wide range for the mineral-derived catalysts (e.g., tunable Cu/Zn ratios and substitution of Cu^{2+}/Zn^{2+} with other divalent ions),[33–35] facilitating further functionalization of the catalysts. The present work demonstrated the design and construction of Cu–ZnO catalysts from some simple mineral precursors, which is a promising direction for catalyst design in selective hydrogenation of bio-derived molecules.

Characterization of catalyst precursors

The different catalyst precursors were prepared via modulating the preset Cu/Zn molar ratios (CuZn-x, x indicates Cu/Zn ratios and inf means infinite). Fig. 1 shows the XRD spectra of the catalyst precursors in the range of 10–40°, which serves as the "fingerprint region" for identification of malachite, rosasite and aurichalcite minerals.[27,29,36] Evident peaks at
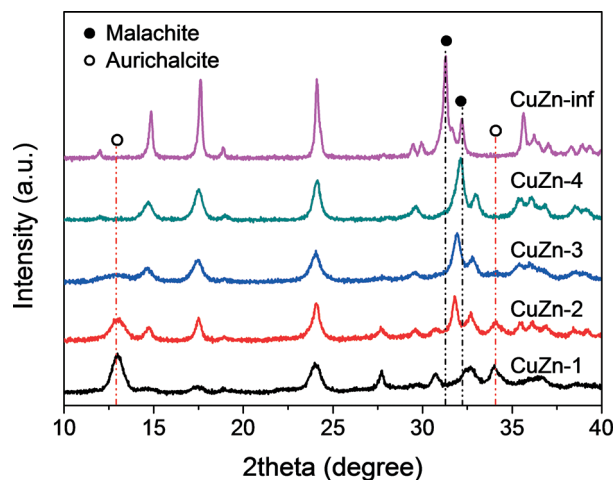

Fig. 1 XRD patterns of the precursors of CuZn-x catalysts.

14.8° (020), 17.6° (120), 24.1° (220), 31.2° (20−1), 32.2° (21−1) and 35.6° (240) were observed for the CuZn-inf precursor, which can be assigned to the characteristic peaks of pure malachite (PDF# 41-1390). Addition of a small amount of Zn^{2+} ions (CuZn-4 and CuZn-3) would lead to a structural change from malachite to rosasite. According to Behrens et al.,[31] the (20−1) and (21−1) diffractions can be employed to distinguish the structural evolution because the decrease in cell volume would proceed when the Cu–O bond is substituted with the Zn–O bond. The peaks at 31.2° (20−1) and 32.2° (21−1) shifted toward higher angles (32.1° and 33.0°) while the peak intensity decreased, indicating the substitution of Cu^{2+} with Zn^{2+} in the lattice and the formation of crystalline rosasite. Further addition of Zn^{2+} (CuZn-2 and CuZn-1) resulted in the continuous decrease of peak intensity and emergence of peaks at 13.0° and 34.3°. The two peaks which appeared belong to the characteristic peaks of aurichalcite (PDF# 17-0743). Only the aurichalcite phase was observed over CuZn-1. Together with the increase of peak width, the intensity of XRD reflections decreased, indicating that the crystallinity of minerals was reduced gradually by the addition of Zn^{2+}. XRD results revealed that pure malachite was produced over CuZn-inf, pure rosasite was formed over CuZn-4 and CuZn-3 and the mixed composite of both rosasite and aurichalcite was observed over CuZn-2 while only aurichalcite could be detected over CuZn-1.

IR spectra allowed visualization of the structure evolutions of the precursors (Fig. 2a and b). The bands in the region of 400–600 cm^{-1} are attributed to Cu–O and/or Zn–O bonds.[28] With the increase of Zn^{2+} content, these bands broadened, shifted to lower frequencies and decreased in intensity. According to Stoilova et al.,[28] this could be attributed to the stronger Cu–O interactions and higher polarization ability of Zn^{2+} ions, indicating the substitution of Cu^{2+} with Zn^{2+} ions. The bands at 712 and 752 cm^{-1} are attributed to the v_4 asymmetric OCO bending modes,[28] which shifted to lower wavenumbers when Cu^{2+} ions were replaced with Zn^{2+} ions. The peak at 820 cm^{-1} is indicative of the v_2 mode of malachite and rosasite, which diminished gradually with the increase of Zn^{2+} content.[29] Furthermore, it is interesting to note that a slight remnant at 820 cm^{-1} was observed over CuZn-1, indicating the existence of a slight amount of rosasite over the sample which is lower than the detection limit of XRD. A new peak at 840 cm^{-1} emerged over CuZn-2 and CuZn-1 which can be attributed to the v_2 mode of aurichalcite. The bands at 970 and 1200 cm^{-1} can also serve as the fingerprint bands of aurichalcite.[28,29] For malachite and rosasite, the bands in the range of 1300–1600 cm^{-1} are attributed to v_4 modes of CO_3^{2-} ions (Fig. 2b). When malachite and rosasite minerals changed to aurichalcite, the bands in this range would be complicated due to the existence of two crystallographically non-equivalent CO_3^{2-} ions bonded to different ions (Cu^{2+} and Zn^{2+}). The band at 1390 cm^{-1} disappeared while the bands at 1370 and 1560 cm^{-1} emerged with the addition of Zn^{2+} ions. The IR results confirmed the structural evolutions of the precursors, as evidenced by XRD results.
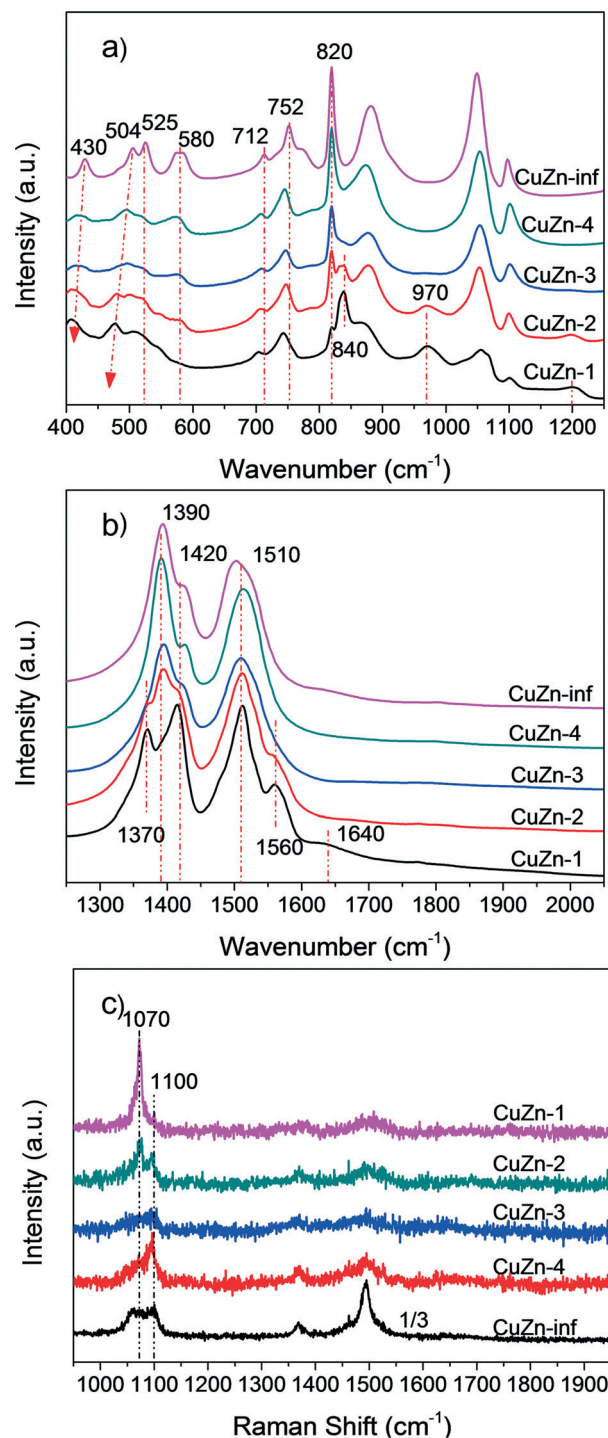

Fig. 2 IR ((a) 400–1250 cm^{-1}, (b) 1250–2050 cm^{-1}) and Raman spectra ((c) intensity of CuZn-inf was divided 3 times) of the CuZn-x precursors.

Raman spectroscopy has been proven to be very useful for studying the mineral precursors (Fig. 2c). The band at 1070 cm^{-1} corresponds to the CO_3^{2-} symmetric stretching mode of aurichalcite while the peak at 1100 cm^{-1} belongs to the rosasite phase.[32,37] For CuZn-2, the overlapped peaks at 1070 and 1100 cm^{-1} were attributed to the mixed crystal phases of aurichalcite and rosasite. A different motif of CuZn-inf was

This journal is © The Royal Society of Chemistry 2015

Catal. Sci. Technol., 2015, 5, 4208–4217 | 4211

observed in the range of 1050–1150 cm^{-1}, which could be ascribed to the overlapped peak of O–H out-of-plane bending and v_1 CO$_3^{2-}$ symmetric stretching modes of malachite.[33,34] Raman results supported the observations of IR experiments.

Characterization of calcined and reduced catalysts

Table 1 gives an overview of the main physicochemical and surface properties of CuZn-x catalysts. The elemental compositions and Cu/Zn molar ratios, determined by ICP experiments, fitted well with the nominal values. CuZn-inf was found to have a surface area (S_{BET}) of ~18 m^2 g^{-1} which was approximately one-third of those for CuZn-x (x = 1, 2, 3, and 4) catalysts. The pore volume (V_p) of CuZn-inf was also lower than those for the other samples. The results indicated that Zn^{2+} tuned the structures of the precursors and the microstructures of the catalysts. The amounts of surface metallic Cu sites (S_{Cu}) and surface acid concentrations (S_{acid}) were determined by N$_2$O and NH$_3$-TPD experiments, respectively. CuZn-inf showed the lowest S_{Cu} and S_{acid}. S_{Cu} increased with the decrease of Cu/Zn molar ratios and reached the maximum at a Cu/Zn ratio of 2. When the Cu/Zn ratio was further decreased, a decrease of S_{Cu} was observed. In contrast, S_{acid} increased monotonously when Cu^{2+} was substituted with Zn^{2+}, indicating that the surface acidity mainly originated from the ZnO component.[38]

Calcination of the precursors resulted in the formation of oxide composites containing an intimate mixture of CuO and ZnO species. Fig. 3 shows the XRD patterns of calcined CuZn-x catalysts. The CuO reflections at 35.6° (002) and 38.7° (111) were broad over all the calcined catalysts, indicating that CuO particles over CuZn-x catalysts were small (PDF# 45-0937). Moreover, the intensity of CuO peaks decreased and the full widths at half maximum of the peaks increased with the addition of Zn^{2+}, demonstrating the decrease of CuO particle sizes and the role of Zn^{2+} in the dispersion of the CuO species. No crystalline ZnO was detected over CuZn-x (2, 3, 4 and inf) catalysts, indicating the high dispersion of ZnO species. Only a weak peak of ZnO at 36.3° (PDF# 36-1451, crystalline size is 9.4 nm) was observed over CuZn-1. Because the diffraction of CuO(002) at 35.6° greatly overlapped with that of ZnO(101), we therefore used the reflection of CuO(111) at 38.7° to quantitatively determine
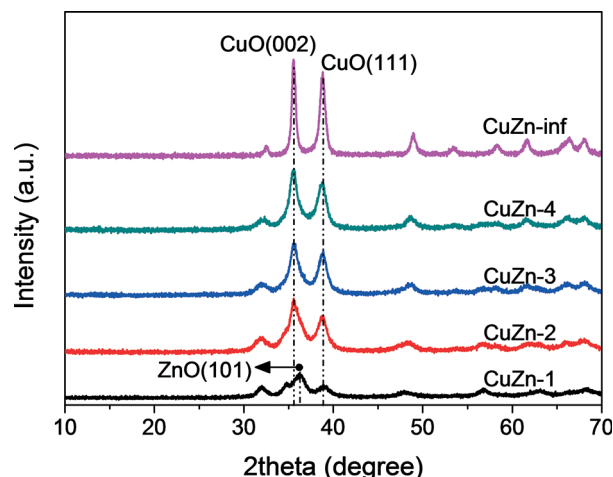

Fig. 3 XRD patterns of the calcined CuZn-x catalysts (CuO, PDF# 45-0937; ZnO, PDF# 36-1451).

the CuO particle sizes (d_{CuO}) (Table 1). The mean CuO crystalline sizes of CuZn-x (x = 1, 2, 3, and 4) were 6.1–7.4 nm, whereas that of CuZn-inf was 11.4 nm. The above results demonstrated that mineral precursors can facilitate the high dispersion of catalyst components. To investigate the reducibility and structural evolutions of the CuZn-x catalysts, TPR experiments were performed (Fig. 4). CuZn-inf exhibited the highest reduction temperature as a result of the CuO crystallites being the largest and poorly porous structures.[39] Concomitantly, the TPR profile of CuZn-inf was different from that of CuZn-x (x = 1, 2, 3, and 4) catalysts, which might be because of the absence of ZnO. The CuZn-x (x = 1, 2, 3, and 4) catalysts all exhibited a broad peak composed of multi-shoulders. With the increase of ZnO content, the peaks of the CuZn-x catalysts shifted slightly towards the lower temperature side, of which CuZn-1 showed the lowest reduction temperature. The results fitted well with the observations of XRD results.[40] For the CuZn-x catalysts, the shoulder at the higher temperature side can be attributed to the reduction of Cu^{2+} species which interacted strongly with ZnO species.[41] The TPR results revealed that the reduction behaviors can also be complicated by the interactions between CuO and ZnO.

The surface acidity of the CuZn-x catalysts was determined by NH$_3$-TPD experiments (Fig. 5). A main peak at 180 °C and

Table 1 The main physicochemical and structural properties of CuZn-x catalysts

Catalysts	Cu content[a] (wt.%)	Zn content[a] (wt.%)	Cu/Zn molar ratios	S_{BET}[b] (m^2 g^{-1})	d_p[b] (nm)	V_p[b] (cm^3 g^{-1})	d_{CuO}[c] (nm)	S_{Cu}[d] (mmol g$_{cat}^{-1}$)	S_{acid}[e] (mmol g$_{cat}^{-1}$)
CuZn-inf	79.6	—	—	18.0	20.7	0.17	11.4	0.39	3.70 × 10^{-4}
CuZn-4	63.8	15.9	4.1	52.4	14.6	0.27	7.4	1.55	6.20 × 10^{-4}
CuZn-3	60.0	19.5	3.2	56.9	12.9	0.25	7.1	2.03	1.06 × 10^{-3}
CuZn-2	53.7	26.3	2.1	55.7	11.5	0.24	6.2	2.12	1.16 × 10^{-3}
CuZn-1	40.3	39.4	1.1	55.8	13.3	0.26	6.1	1.78	1.27 × 10^{-3}

[a] Determined by ICP experiments. [b] Determined by N$_2$ adsorption experiments. [c] Calculated by using the CuO(111) reflection at 38.7° based on the Scherrer equation. [d] The amounts of surface metallic Cu sites (S_{Cu}) were determined by N$_2$O titration measurements. [e] The surface acid concentrations (S_{acid}) were determined by NH$_3$-TPD measurements.
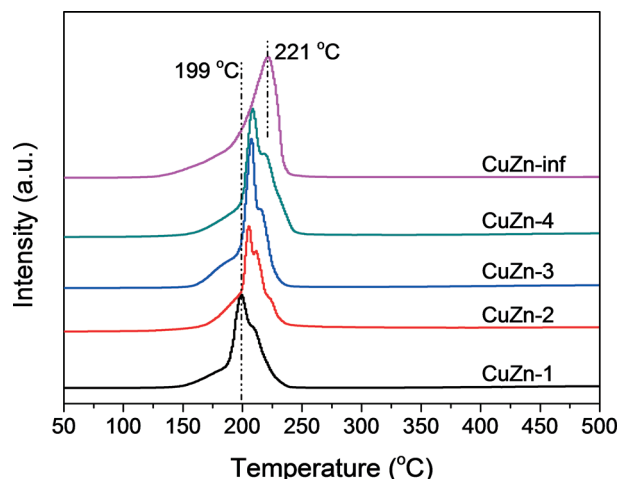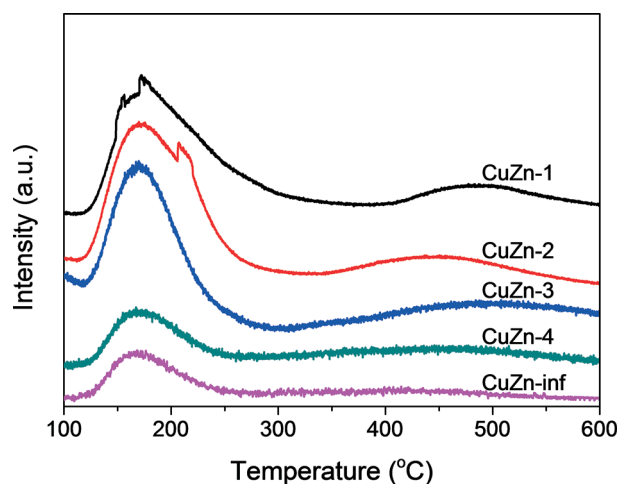
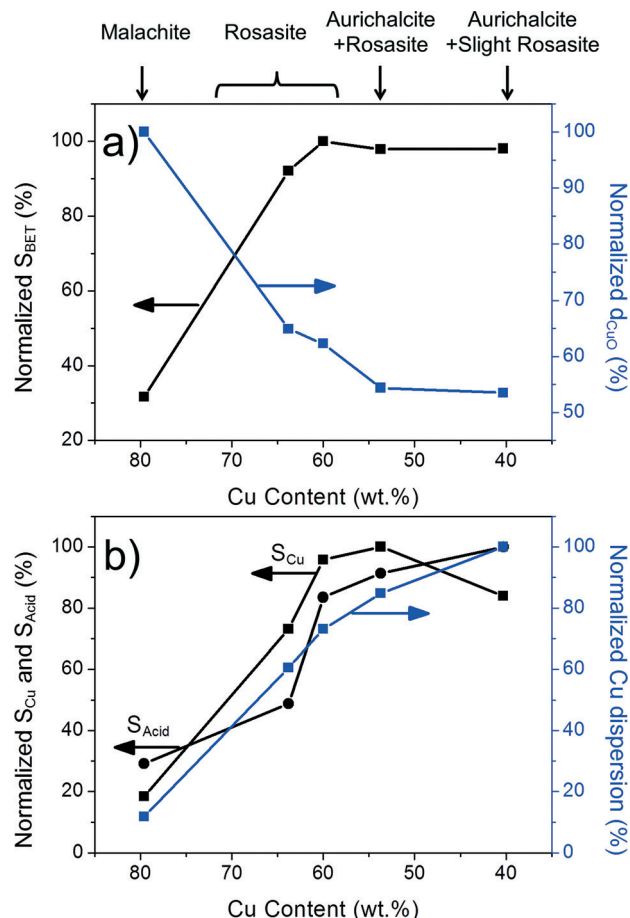**Fig. 4** TPR results of the calcined CuZn-x catalysts.

Fig. 6 Correlations between the main physicochemical properties (a, normalized S_{BET} and d_{CuO}; b, normalized S_{Cu}, S_{acid} and Cu dispersion) and Cu contents of CuZn-x catalysts (normalized: the highest is 100%).

a small one in the range of 400–500 °C were observed for all the catalysts, which can be ascribed to the weak and strong acid sites, respectively. The amounts of surface acid sites were enhanced when the Zn^{2+} content was increased. We calculated the amounts of surface acid sites (Table 1) and found that the CuZn-1 catalyst exhibited the highest surface acid concentration (1.27×10^{-3} mmol g_{cat}^{-1}) while CuZn-inf only possessed slight surface acidity (3.70×10^{-4} mmol g_{cat}^{-3}). The results indicated that the surface acidity mainly originated from the ZnO species.[38] It should be noted that all the catalysts exhibited relatively low densities of surface acidity (about 3 orders lower than S_{Cu}), mainly due to the fact that ZnO is an oxide with low surface acidity. The moderate surface acid sites would facilitate the tunable production of DHMF and DMF under different conditions, which would be discussed in the following sections.

Fig. 6 illustrated the correlations between Cu contents, mineral structures and main structural and surface properties of the CuZn-x catalysts. When Cu^{2+} ions were replaced with Zn^{2+} ions, the precursor structures evolved from

malachite to rosasite, and then changed to a mixture of rosasite and aurichalcite phases, which brought about the different properties of the resulting catalysts. As shown in Fig. 6a, addition of Zn^{2+} ions increased the S_{BET} of the calcined catalysts by ~3 times and decreased the mean CuO particle size by approximately 0.5 times. Cu dispersion increased with the decrease of Cu content, which resulted in a comprehensive volcano trend of the surface metallic Cu concentration (Fig. 6b). CuZn-2 displayed the highest amount of surface Cu sites. In contrast, the amount of surface acid sites increased with the decrease of Cu content, indicating that ZnO species may be responsible for the surface acidity.

Performance of CuZn-x catalysts for DHMF synthesis

The selective hydrogenation of HMF to DHMF over CuZn-x catalysts was conducted at 100 °C and 1.5 MPa for 1 h. The performance of the CuZn-x catalysts was screened (Table 2). The commercial RANEY® metal (Ni, Co and Cu) catalysts were also employed as references. A low HMF conversion of ~16.3% was obtained over CuZn-inf. With the decrease of Cu/Zn ratios, HMF conversion first increased, reached a maximum of 83.5% over the CuZn-2 catalyst and then decreased, while DHMF selectivity was almost constant around 99%. The

Fig. 5 NH$_3$-TPD results of the calcined CuZn-x catalysts.

Table 2 HMF hydrogenation over CuZn–*x* catalysts and commercial RANEY® metals at 100 °C[a]

Catalysts	Conv. (%)	Sel. (%)		
		DHMF	DHMTHF	Others[b]
CuZn-inf	16.3	98.1	0	1.9
CuZn-4	34.1	97.9	0	2.1
CuZn-3	75.4	98.9	0	1.1
CuZn-2	83.5	99.1	0	0.9
CuZn-1	75.3	99.2	0	0.8
RANEY® Cu	60.0	98.9	0	1.1
RANEY® Co	63.9	97.2	2.7	1.2
RANEY® Ni	73.1	69.5	20.1	10.4

[a] Conditions: 1.5 MPa, 1 h, catalyst 0.5 g, HMF 1.5 g. [b] Others mainly include DMF and 5-methylfurfuryl alcohol (MFA).

activity follows the similar trend of surface metallic Cu concentration (Fig. S1†). Interestingly, CuZn-1 and CuZn-3 possessed different surface metallic Cu concentration, but showed similar activity towards HMF hydrogenation to DHMF. According to Morrison *et al.*,[42] acids can help in the activation of carbonyl groups and thus facilitate the reactivity. The similar reactivity of CuZn-1 and CuZn-3 can be attributed to the synergy between surface metallic Cu sites and acid sites. The results revealed that ZnO not only dispersed Cu sites but also provided some acid sites for promoting HMF hydrogenation. It should be noted that bare ZnO without metallic Cu sites can hardly catalyze HMF hydrogenation in our cases, as evidenced by model tests (Table S1†).

The effectiveness of the CuZn-2 catalyst was also compared with that of commercial RANEY® Cu, Co and Ni catalysts under the same reaction conditions. Among the RANEY® metals, RANEY® Ni exhibited the highest activity with a HMF conversion of 73.1%, which was still lower than that for the CuZn-2 catalyst. The superior performance of the CuZn-2 catalyst indicated that mineral precursors could facilitate the formation of highly dispersed metal sites and high catalytic activity. Moreover, the DHMF selectivity of RANEY® Ni was much lower than that of the CuZn-2 catalyst, mainly due to the formation of DHMTHF. DHMTHF is formed by ring hydrogenation of DHMF. Thus, the formation of DHMTHF over RANEY® Ni indicates the relatively strong C=C hydrogenation ability of Ni, which is detrimental to DHMF synthesis.[17] In contrast, CuZn-*x* and RANEY® Cu catalysts exhibited high selectivity to DHMF, indicating that the catalysts have high reactivity to C=O bonds while having relatively low reactivity toward C=C hydrogenation. Extensive studies regarding the configuration of adsorbed aldehydes have been conducted over the Cu surface. The $\eta^1(O)$ configuration is known to be formed;[43,44] thus, Cu-based catalysts could exhibit high selectivity to C=O hydrogenation. The above results confirmed that mineral-derived Cu-based catalysts are good candidates for selective hydrogenation of HMF to DHMF.

The time course of the CuZn-2 catalyst at 100 °C and 1.5 MPa was studied to determine the highest reactivity and DHMF yield. As plotted in Fig. 7, HMF conversion increased from 83.5% to 100% upon increasing the reaction time from 1 h to 2 h, while the selectivity was almost unchanged. Further increase of reaction time (up to 20 h) had little effect on DHMF selectivity. The performance of the CuZn-*x* catalysts at 100 °C for 20 h was also compared (Fig. S2†), which all exhibited high DHMF yields. Very slight amounts of hydrogenolysis and ring-saturation by-products (MFA, DMF and DHMTHF) were detected under the conditions. The results revealed the high selectivity of Cu–ZnO catalysts towards synthesis of DHMF at 100 °C.

Selective conversion of HMF to DMF

Selective hydrogenation of HMF to DMF involves the hydrogenation of the C=O bond and hydrogenolysis of C–O bonds, which is a more challenging reaction than DHMF synthesis. DHMF is the main intermediate of DMF over Cu catalysts while 2,5-dimethyltetrahydrofuran (DMTHF) is the over-hydrogenated product.[20]

DHMF was already obtained effectively over the CuZn-2 catalyst at 100 °C. The hydrogenolysis of C–O bonds would be significantly promoted by elevation of reaction temperatures, as reported in previous studies.[17,20] The effect of reaction temperature on the performance of the CuZn-2 catalyst was therefore studied (Table 3). At 80 °C, 53.7% of HMF was converted into DHMF with ~99.5% selectivity. The conversion increased to 83.5% when the temperature was elevated to 100 °C and the DHMF selectivity was maintained around 99%. With a further increase of reaction temperature to 140 °C, HMF was almost totally converted while DHMF selectivity dropped due to the formation of MFA and DMF. Further increasing the reaction temperature tuned the product distribution dramatically. DHMF selectivity decreased, whereas MFA and DMF selectivity increased monotonously. The best DMF selectivity of ~40.6% was obtained at 220 °C. Moreover,
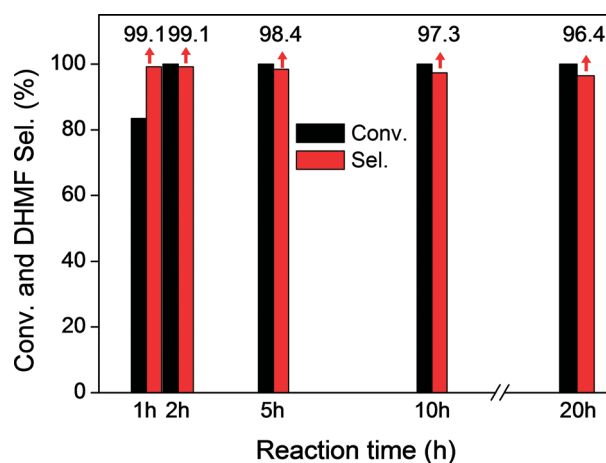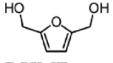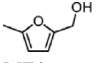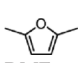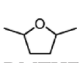

Fig. 7 Time course of catalytic performance of the CuZn-2 catalyst at 100 °C (1.5 MPa H$_2$, HMF 1.5 g, catalyst 0.5 g).

4214 | *Catal. Sci. Technol.*, 2015, **5**, 4208–4217

This journal is © The Royal Society of Chemistry 2015

Table 3 Influence of reaction temperature on HMF hydrogenation over CuZn-2 catalyst[a]

T (°C)	Conv. (%)	Sel. (%)				
		DHMF	MFA	DMF	DMTHF	Others
80	53.7	99.5	0	0	0	0.5
100	83.5	99.1	0.2	0	0	0.7
140	97.5	94.4	3.6	1.8	0	0.2
180	100	50.0	20.9	27.4	1.6	0.1
220	100	33.1	24.1	40.6	1.9	0.3

[a] Conditions: 1.5 MPa, 1 h, catalyst 0.5 g, HMF 1.5 g.

DHMF and MFA were obtained with a total yield of 57.2%, which could be converted to DMF by hydrogenolysis of the side –CH$_2$OH group.[17] In summary, the results showed that high reaction temperatures would promote C–O hydrogenolysis reactions, while the DMF yield could be further improved. Therefore, 220 °C was chosen to further optimize the DMF selectivity. The above results facilitated the potentially tunable synthesis of DMF and DHMF over the Cu–ZnO catalysts.

Fig. 8 showed the time course of catalytic performance of the CuZn-2 catalyst at 220 °C and 1.5 MPa. Upon increasing the reaction time from 1 h to 2 h, the DMF yield did not change dramatically, whereas DHMF yield decreased with the elevation of MFA yield. After 5 h reaction time, DHMF and MFA were almost totally consumed, giving rise to a high DMF yield of 91.8%, which indicates that C–O hydrogenolysis was promoted. Upon further increase in reaction time, DMF selectivity decreased slightly due to the formation of DMTHF. Nevertheless, DMF selectivity was maintained at a high level under our reaction conditions.

The above results revealed a reaction pathway for HMF hydrogenation under the reaction conditions. HMF was initially hydrogenated to DHMF (Fig. 7). Upon increasing the
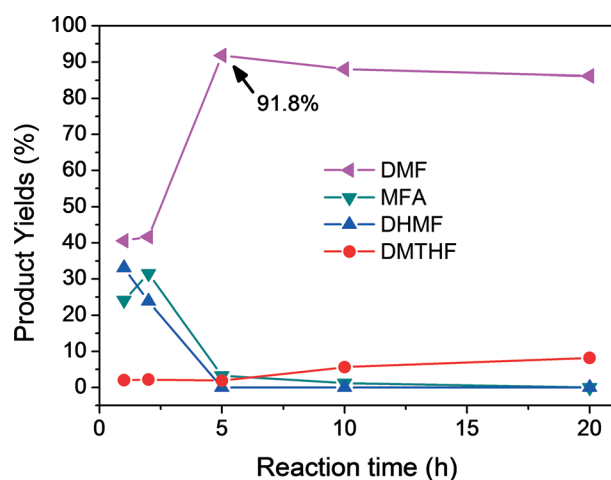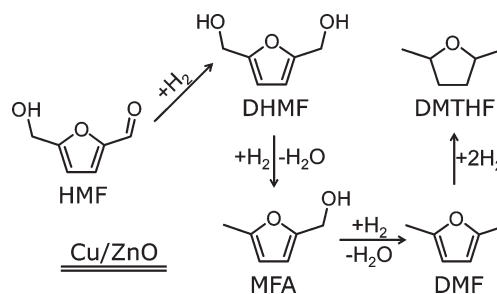
reaction temperature, the generated DHMF was converted, whereas MFA, DMF and a very slight amount of DMTHF were formed (Table 3). When the reaction time was increased, DHMF was continuously converted (Fig. 8). In contrast, MFA was first formed and then converted, whereas DMF was formed substantially. The yield of DMTHF increased slightly when the reaction time was increased. The reaction pathway is summarized in Scheme 3.

The above results demonstrate the tunable and highly selective conversion of HMF to DHMF or DMF using a binary mineral-derived Cu–ZnO catalyst under different conditions (Scheme 1), confirming the potential of non-noble Cu catalysts for selective hydrogenation of HMF. Key to our success is the highly dispersed active sites, well-controlled surface acidity and suitable reaction conditions.

Catalyst stability

HMF hydrogenation to DMF was chosen to further investigate the reusability of the CuZn-2 catalyst due to the relatively severe conditions (220 °C). A sharp decrease of HMF conversion and DMF selectivity was observed (Fig. 9a), indicating that the catalyst deactivated during the tests. Thermogravimetry (TG) experiments of fresh reduced and used CuZn-2 catalysts were performed to examine the deposition of carbonaceous species (Fig. 9b and c). The weight of fresh reduced CuZn-2 increased, which could be ascribed to the oxidation of Cu. In contrast, the dramatic weight loss of used CuZn-2 accompanied by a sharp exothermic peak revealed the oxidization of carbonaceous species.[18] The carbonaceous species can be strongly adsorbed on the catalyst and hinder the activity.[19] The XRD patterns revealed that Cu particles were not evidently grown after 5 runs (Fig. S3†). Besides, the recovery processes (e.g., washing) would inevitably cause weight loss of the catalyst. The results suggested that deactivation of CuZn-2 mainly resulted from deposition of carbonaceous species, which was consistent with previous reports.[14,18] The slight Cu particle growth and weight loss of the catalyst may also cause the loss of reactivity to some extent. The deposited carbonaceous species can be removed by re-calcination and re-reduction procedures.[14,45] Besides, design of an efficient catalyst that can catalyze HMF hydrogenolysis at low temperatures can promote the stability due to the minimization of humin formation.

Fig. 8 Time course of catalytic performance of the CuZn-2 catalyst at 220 °C (1.5 MPa H$_2$, HMF 1.5 g, catalyst 0.5 g).

Scheme 3 Reaction pathway of HMF hydrogenation under the conditions.

This journal is © The Royal Society of Chemistry 2015

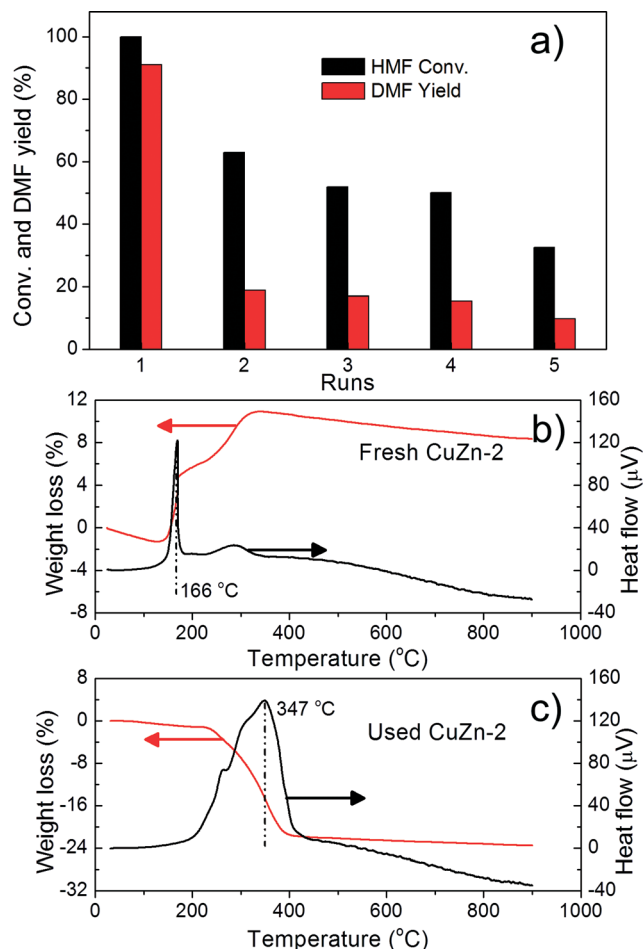Catal. Sci. Technol., 2015, 5, 4208–4217 | 4215

Fig. 9 (a) Reusability of the CuZn-2 catalyst for DMF synthesis from HMF hydrogenation (conditions: 220 °C, 1.5 MPa, 5 h, HMF 1.5 g, catalyst 0.5 g, 1,4-dioxane 35 ml). (b) Thermogravimetry (TG) spectra of fresh reduced CuZn-2 catalyst. (c) TG spectra of used CuZn-2 catalyst.

Applications in conversion of bio-derived molecules

The CuZn-2 catalyst was further extended to selective hydrogenation of other bio-derived furan molecules (5-methylfurfural and furfural). As shown in Table 4, MFA and DMF were obtained with high yields of 99.2% and 91.6%, respectively, under different reaction conditions when 5-methylfurfural was employed as the reactant. For selective hydrogenation of furfural, high yields of

furfuryl alcohol (98.9%) and 2-methylfuran (94.5%) were also achieved through tuning of the reaction conditions. These results further demonstrated the great flexibility of mineral-based Cu–ZnO catalysts for efficiently and selectively converting bio-derived molecules. Further improvement and rational design of mineral-derived Cu catalysts are in progress.

Conclusions

The non-noble mineral-derived (malachite, rosasite and aurichalcite) Cu–ZnO catalysts prepared by a simple controlled co-precipitation method have been demonstrated to have high reactivity and selectivity for the conversion of HMF to either DHMF (~99.1% yield) or DMF (~91.8% yield). The tunable synthesis of both products was achieved by simply tuning the reaction temperature and reaction time. The structural evolutions of minerals and structure–performance relationships were elucidated by various characterization techniques based on the composition and structural and surface properties, and catalyst tests. The Cu–ZnO catalyst derived from the mixture of rosasite and aurichalcite (CuZn-2) was found to possess the highest reactivity, which is due to its surface Cu concentration being the highest, suitable acidity and good microstructures. The results here are expected to be useful for further rational design of earth-abundant Cu catalysts. The catalyst was also extended to selective hydrogenation of other bio-derived molecules (furfural and 5-methylfurfural) to valuable products, demonstrating the flexibility of Cu catalyst for biomass conversion.

Acknowledgements

Notes and references

1   R. J. van Putten, J. C. van der Waal, E. de Jong, C. B. Rasrendra, H. J. Heeres and J. G. de Vries, *Chem. Rev.*, 2013, **113**, 1499–1597.
2   J. N. Chheda, G. W. Huber and J. A. Dumesic, *Angew. Chem., Int. Ed.*, 2007, **46**, 7164–7183.
3   C. Zeng, H. Seino, J. Ren, K. Hatanaka and N. Yoshie, *Polymer*, 2013, **54**, 5351–5357.
4   C. Zeng, H. Seino, J. Ren, K. Hatanaka and N. Yoshie, *Macromolecules*, 2013, **46**, 1794–1802.
5   C. Zeng, H. Seino, J. Ren and N. Yoshie, *ACS Appl. Mater. Interfaces*, 2014, **6**, 2753–2758.
6   M. Chatterjee, T. Ishizaka and H. Kawanami, *Green Chem.*, 2014, **16**, 4734–4739.
7   Y. Roman-Leshkov, C. J. Barrett, Z. Y. Liu and J. A. Dumesic, *Nature*, 2007, **447**, 982–985.
8   P. T. Do, J. R. McAtee, D. A. Watson and R. F. Lobo, *ACS Catal.*, 2013, **3**, 41–46.
9   Y.-P. Li, M. Head-Gordon and A. T. Bell, *J. Phys. Chem. C*, 2014, **118**, 22090–22095.

Table 4 Applications of CuZn-2 catalyst in the conversion of furanic compounds

Feedstock	Conditions[a]	Conv. (%)		Sel. (%)
	100 °C, 2 h	100	(furfuryl alcohol structure) OH	99.2
	220 °C, 10 h	100	(methylfuran structure)	91.6
	100 °C, 2 h	100	(furfuryl alcohol structure) OH	98.9
	220 °C, 10 h	100	(2-methylfuran structure)	94.5

[a] 1.5 MPa, catalyst 0.5 g, feedstock 1.5 g.

10 R. Alamillo, M. Tucker, M. Chia, Y. Pagan-Torres and J. Dumesic, *Green Chem.*, 2012, **14**, 1413–1419.

11 J. Ohyama, A. Esaki, Y. Yamamoto, S. Arai and A. Satsuma, *RSC Adv.*, 2013, **3**, 1033–1036.

12 J. Mitra, X. Zhou and T. Rauchfuss, *Green Chem.*, 2015, **17**, 307–313.

13 M. Tamura, K. Tokonami, Y. Nakagawa and K. Tomishige, *Chem. Commun.*, 2013, **49**, 7034–7036.

14 J. Jae, W. Zheng, R. F. Lobo and D. G. Vlachos, *ChemSusChem*, 2013, **6**, 1158–1162.

15 Y. Zu, P. Yang, J. Wang, X. Liu, J. Ren, G. Lu and Y. Wang, *Appl. Catal., B*, 2014, **146**, 244–248.

16 G. H. Wang, J. Hilgert, F. H. Richter, F. Wang, H. J. Bongard, B. Spliethoff, C. Weidenthaler and F. Schuth, *Nat. Mater.*, 2014, **13**, 293–300.

17 X. Kong, Y. Zhu, H. Zheng, F. Dong, Y. Zhu and Y.-W. Li, *RSC Adv.*, 2014, **4**, 60467–60472.

18 X. Kong, R. Zheng, Y. Zhu, G. Ding, Y. Zhu and Y.-W. Li, *Green Chem.*, 2015, **17**, 2504–2514.

19 Y. B. Huang, M. Y. Chen, L. Yan, Q. X. Guo and Y. Fu, *ChemSusChem*, 2014, **7**, 1068–1072.

20 A. J. Kumalaputri, G. Bottari, P. M. Erne, H. J. Heeres and K. Barta, *ChemSusChem*, 2014, **7**, 2266–2275.

21 T. S. Hansen, K. Barta, P. T. Anastas, P. C. Ford and A. Riisager, *Green Chem.*, 2012, **14**, 2457.

22 Y. Nakagawa, K. Takada, M. Tamura and K. Tomishige, *ACS Catal.*, 2014, **4**, 2718–2726.

23 E. R. Sacia, M. Balakrishnan and A. T. Bell, *J. Catal.*, 2014, **313**, 70–79.

24 Y. Zhu, X. Kong, D.-B. Cao, J. Cui, Y. Zhu and Y.-W. Li, *ACS Catal.*, 2014, **4**, 3675–3681.

25 E. S. Vasiliadou, T. M. Eggenhuisen, P. Munnik, P. E. de Jongh, K. P. de Jong and A. A. Lemonidou, *Appl. Catal., B*, 2014, **145**, 108–119.

26 H. Tan, M. N. Hedhill, Y. Wang, J. Zhang, K. Li, S. Sioud, Z. A. Al-Talla, M. H. Amad, T. Zhan, O. E. Tall and Y. Han, *Catal. Sci. Technol.*, 2013, **3**, 3360.

27 B. Bems, M. Schur, A. Dassenoy, H. Junkes, D. Herein and R. Schlögl, *Chem. – Eur. J.*, 2003, **9**, 2039–2052.

28 D. Stoilova, V. Koleva and V. Vassileva, *Spectrochim. Acta, Part A*, 2002, **58**, 2051–2059.

29 M. Behrens, F. Girgsdies, A. Trunschke and R. Schlögl, *Eur. J. Inorg. Chem.*, 2009, **2009**, 1347–1357.

30 M. Behrens, *J. Catal.*, 2009, **267**, 24–29.

31 M. Behrens and F. Girgsdies, *Z. Anorg. Allg. Chem.*, 2010, **636**, 919–927.

32 R. L. Frost, M. C. Hales and B. Jagannadha Reddy, *Polyhedron*, 2007, **26**, 3291–3300.

33 R. L. Frost, D. L. Wain, W. N. Martens and B. J. Reddy, *Spectrochim. Acta, Part A*, 2007, **66**, 1068–1074.

34 R. L. Frost, *J. Raman Spectrosc.*, 2006, **37**, 910–921.

35 R. L. Frost, B. J. Reddy, D. L. Wain and W. N. Martens, *Spectrochim. Acta, Part A*, 2007, **66**, 1075–1081.

36 S. Zander, E. L. Kunkes, M. E. Schuster, J. Schumann, G. Weinberg, D. Teschner, N. Jacobsen, R. Schlögl and M. Behrens, *Angew. Chem., Int. Ed.*, 2013, **52**, 6536–6540.

37 R. L. Frost, W. N. Martens, L. Rintoul, E. Mahmutagic and J. T. Kloprogge, *J. Raman Spectrosc.*, 2002, **33**, 252–259.

38 Y. Zhu, X. Kong, X. Li, G. Ding, Y. Zhu and Y.-W. Li, *ACS Catal.*, 2014, **4**, 3612–3620.

39 Y. Zhu, Y. Zhu, G. Ding, S. Zhu, H. Zheng and Y. Li, *Appl. Catal., A*, 2013, **468**, 296–304.

40 L. Shi, C. Zeng, Y. Jin, T. Wang and N. Tsubaki, *Catal. Sci. Technol.*, 2012, **2**, 2569.

41 J. Agrell, K. Hasselbo, K. Jansson, S. G. Järås and M. Boutonnet, *Appl. Catal., A*, 2001, **211**, 239–250.

42 R. Morrison and R. Boyd, *Organic Chemistry*, Prentice Hall, Englewood Cliffs, NJ, 6th edn, 1992.

43 S. Sitthisa, T. Sooknoi, Y. Ma, P. B. Balbuena and D. E. Resasco, *J. Catal.*, 2011, **277**, 1–13.

44 Y. Nakagawa, H. Nakazawa, H. Watanabe and K. Tomishige, *ChemCatChem*, 2012, **4**, 1791–1797.

45 B. J. O'Neill, D. H. Jackson, A. J. Crisci, C. A. Farberow, F. Shi, A. C. Alba-Rubio, J. Lu, P. J. Dietrich, X. Gu, C. L. Marshall, P. C. Stair, J. W. Elam, J. T. Miller, F. H. Ribeiro, P. M. Voyles, J. Greeley, M. Mavrikakis, S. L. Scott, T. F. Kuech and J. A. Dumesic, *Angew. Chem., Int. Ed.*, 2013, **52**, 13808–13812.

This journal is © The Royal Society of Chemistry 2015

Catal. Sci. Technol., 2015, **5**, 4208–4217 | **4217**